Article

Influence of the Machining Process on the Wear Properties of Self-Mated Structural Steel in Dry Sliding Conditions

Gian Luca Garagnani [ID], Enrico Baroni *, Annalisa Fortini [ID], Luciano D'Angelo and Mattia Merlin [ID]

Department of Engineering (DE), University of Ferrara, 44121 Ferrara, Italy; gian.luca.garagnani@unife.it (G.L.G.); annalisa.fortini@unife.it (A.F.); luciano.dangelo@unife.it (L.D.); mattia.merlin@unife.it (M.M.)
* Correspondence: enrico.baroni@unife.it

Abstract: This work investigates the tribological behavior of a machined S355JR structural steel in dry sliding conditions for the development of an innovative seismic dissipation system. Flat-ended pins and disks were made of the same structural steel to simulate the conformal contact of different device parts. Pins were machined by turning, while disks were milled and turned to obtain a nominal average surface Ra roughness ranging from 0.8 µm to 6.3 µm. The influence of the surface roughness on the coefficient of friction (COF), specific wear rate (SWR), and time to steady-state (TSS) was investigated. Tribological tests were conducted reciprocating motion in dry sliding conditions to simulate the operating conditions of the device, with 1 Hz and 2 Hz reciprocating frequencies and an applied normal load of 50 N. The Rsk and Rku roughness parameters helped to better understand the tribological response of milled and turned disks, having an influence on the TSS and SWR.

Keywords: roughness; machining; friction; wear; running-in; structural steel

1. Introduction

The seismic retrofitting of existing structures is critical in earthquake-prone regions, driving the development of cost-effective and efficient systems to prevent structural damage during seismic events. Passive Energy Dissipation (PED) devices, such as Friction Dampers (FDs), are widely used for their ability to enhance energy dissipation. FDs, comprising plates connected by bolts, use friction pads to dissipate energy and represent one of the simplest and most economical options [1].

Within this context, tribological issues are essential in defining the design, performance, and operating life of components and systems. The increasing need for enhanced reliability and efficiency in components, coupled with the imperative to reduce frictional losses and achieve higher power density, has raised the tribological requirements on contact surfaces. Surface engineering techniques, as well as coatings and lubricant approaches, have been widely studied and adopted to decrease friction and wear [2–4]. Surface texturing is a surface engineering technique to reduce friction, as highlighted by several studies [5–8]. To accurately characterize the tribological behavior of a friction damper and obtain reliable results for the coefficient of friction (COF) trends and specific wear rate (SWR), testing conditions that replicate real-world scenarios are crucial. In this context, the tribological behavior of brake systems closely resembles that of FDs. Recently, Sinha et al. [9] highlighted that Pin on Disk (PoD) tests offer an economical and efficient method to replicate several tribological scenarios since the tribometer's versatile settings enable the adjustment of relevant parameters.

The role of initial roughness on friction and wear processes has been widely investigated in prior studies [10–14]. Some research has also dealt with predicting wear resistance based on the relationship between the surface texture roughness parameters and the wear resistance [15–18]. It is worth noting that, depending on the specific tribo-couple, the optimal surface roughness leads to minimum wear. It has been reported [10,13] that higher

initial roughness parameters promote extended steady-state periods and reduced coefficient of friction, whereas smooth surfaces show higher COF values [12]. Additionally, higher initial roughness surfaces result in a higher wear rate [10]. For steel substrates, the role of surface preparation on roughness parameters, and the effects on friction and wear, Sedlaček et al. [12] analyzed through dry and lubricated PoD tests the role of different average surface roughness on 100Cr6 steel plates prepared by grinding, polishing, turning, and milling. They reported that the COF is lower for dry tests when roughness is higher and the sliding distance to steady-state tends to become longer with an increase in roughness. In a subsequent study, Sedlaček et al. [11] investigated the influence of surface roughness parameters on the tribological behavior of contact surfaces under dry and boundary contact sliding. The results indicated that standard roughness parameters, i.e., average surface roughness (Sa) and root square (Sq), are insufficient to determine the tribological properties of contact surfaces. Additionally, skewness (Ssk) and kurtosis (Sku) showed a good correlation to the tribological properties and could be used for planning surfaces and surface roughness with the desired tribological behavior in boundary lubrication regimes. More recently, Liang et al. [13] explored the role of initial roughness parameters on the initial steady wear transition time, wear loss, and deformation in the subsurface, finding that higher initial values of Ra (arithmetic mean of the absolute values of the roughness profile ordinates), Rq (root mean square height of the profile), and Rku (kurtosis) result in a larger average friction coefficient and a longer initial steady wear transition period. Moreover, for initial roughness values below a specific limit (Ra in the range of 0.3–0.5 μm and Rq in the range of 0.1–0.4 μm), the weight and the volume loss remained relatively consistent. Some studies were also focused on the influence of machining processes [19,20]. Ba et al. [20] analyzed the role of the Rsk and Rku roughness parameters of steel surfaces machined by milling and turning to examine how the texture's characteristics influence the tribological behavior in the sliding direction of friction tests. More specifically, they reported that abrasion was the predominant wear mechanism on milled surfaces, with plowing oriented toward relative movement. Conversely, on a turned surface, regions of plastic deformation aligned with the sliding direction of the pin and crater formations were observed. These authors suggested that the milled surface exhibited a better tribological performance compared to the turned one.

Based on the outcomes of the above-reported literature, the present study analyzes the effect of the surface topography on the dry-sliding wear behavior of a structural steel under self-mating test conditions. The investigation is driven by the development of a novel passive energy dissipation device for seismic applications whose characteristics were explored in previous works [21,22]. Specifically, previous analyses [21] were devoted to analyzing the tribological behavior of the S355JR structural steel preliminarily treated by different mechanical and galvanic processes, i.e., electrolytic nickel plating, white electrolytic zinc plating, and two shot-peening treatments. The experimental findings reveal the limitations of electrolytic nickel plating and shot-peening treatments in terms of steady-state stage, reaching COFst values similar to that of the TR reference condition in less than two minutes. Additionally, electrolytic zinc plating treatment shows a significant improvement with respect to the turned surface tribological behavior despite the decrement in the overall COF's steadiness with repetition and sliding time increments.

The paper begins with a review of the literature on the effect of surface properties in the tribological performance of contact surfaces, focusing on the role of roughness in affecting the coefficient of friction and specific wear rate (SWR) data in the tribological performance of self-mating materials. Section 2 describes the materials and the machining process adopted to analyze the effect of the surface roughness on the tribological behavior, tested by dry-sliding wear tests under reciprocating motion. Section 3 summarizes and discusses the experimental findings regarding the COF, SWR, and running-in duration outcomes, together with their relation to the turned and milled surfaces.

The main contribution of this paper lies in its innovative approach to studying the operating conditions of a novel passive energy dissipation device through lab-scale testing.

Unlike previous works, this study focuses specifically on the influence of surface properties on tribological behavior and the resulting steady-state regime. By analyzing these factors, the paper provides new insights and guidelines for optimizing surface roughness and managing the running-in period during the development of friction damper devices. This research differs from similar works by offering a detailed investigation into the interplay between surface characteristics and device performance, which has not been extensively explored in the literature.

2. Materials and Methods

The material used in this investigation was a commercially available S355JR structural steel whose chemical composition (wt.%), determined by the Glow Discharge Optical Emission Spectroscopy (GDOES, Spectruma Analytik GDS 650, Hof, Germany) technique, is reported in Table 1. S355JR steel flat-ended cylindrical pins and disks were employed to study the influence of surface preparation on the tribological behavior in dry-sliding conditions.

Table 1. Chemical composition (wt.%) of the analyzed S355JR steel.

	Chemical Composition (wt.%)—Fe Balance							
	C	**Si**	**Mn**	**P**	**S**	**Cu**	**N**	**Fe**
Average	0.233	0.362	1.233	0.012	0.036	0.410	0.010	Balance
St. Dev.	0.015	0.014	0.093	0.001	0.013	0.023	0.002	

From the commercially available S355 JR steel plate, n. 8 disks were machined: n. 4 disks were milled and n. 4 disks were turned to obtain increasing nominal average surface roughness (Ra) ranging from 0.8 μm to 6.3 μm. The milled disks were labeled as M1, M2, M3, and M4, whereas the turned disks were labeled as T1, T2, T3, and T4. The corresponding targeted Ra values for both M and T disks were 0.8 μm, 1.6 μm, 3.2 μm, and 6.3 μm. Concerning the pins, they were machined by turning with a nominal average surface roughness equal to 0.8 μm. A total of n. 80 pins were involved in the tribological campaign. The surface properties of the machined disks were evaluated through a Talysurf CCI Lite non-contact 3D optical profilometer (Taylor-Hobson, Leicester, UK) with an optical resolution of 0.76 μm. For each of the investigated n. 8 disks, five replicas were made to obtain the average values of the linear roughness parameters Ra (arithmetic average height), Rq (root mean square roughness), Rz (ten point height), Rsk (skewness), and Rku (kurtosis), according to the ISO 4287 standard [23]. The measured Ra roughness values were then evaluated and compared to the targeted ones.

The Vickers hardness of the S355JR steel was measured and reported in the previous work from the authors and resulted equal to 228 ± 45 [21]. Wear tests were performed at room temperature by a TR-20LE tribometer (Ducom Instruments, Bangalore, India) in pin-on-disks configuration (ASTM G99-17 standard [24]), with reciprocating sliding condition. The above-mentioned turned and milled disks were 165 mm in diameter, while the flat-ended pins were 6 mm in diameter. According to [22], tests were conducted under an applied load of 50 N and at 1 Hz and 2 Hz oscillatory frequencies (i.e., linear sliding speeds of 0.111 m/s and 0.222 m/s, respectively) to reproduce the actual condition of the friction damper device. Before the wear tests, the specimens were cleaned in an ultrasonic bath with isopropanol. Tests were run at room temperature and in dry conditions on an average 56 mm circular arc wear track. The WINDUCOM-2000™ (Ducom, Bangalore, India) data logging software was employed to continuously record the frictional force by a load cell. In Figure 1, a representative picture of the test set-up is reported.
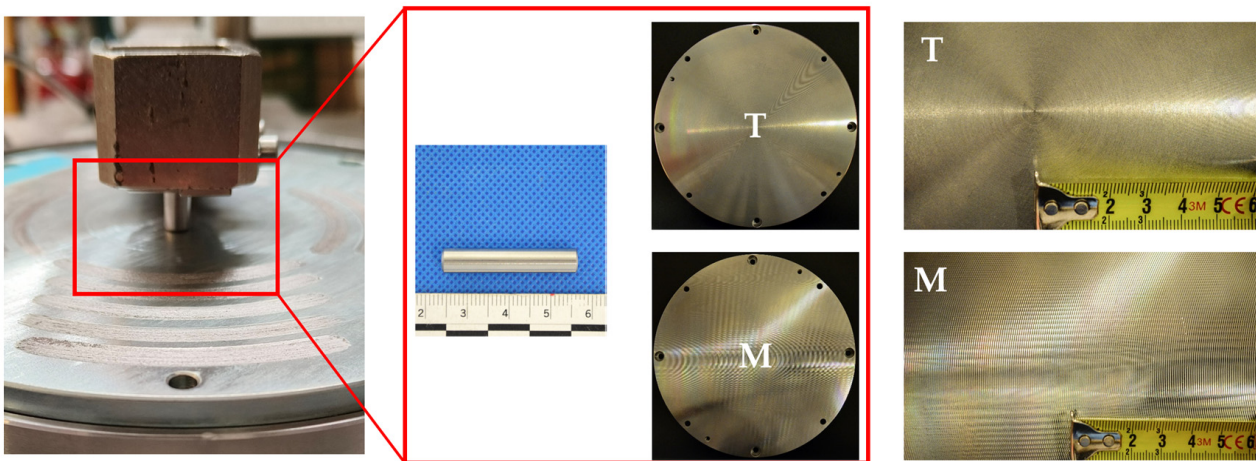
Figure 1. Schematic picture of the wear test set-up and the specimens involved.

Regarding the experimental wear test campaign, preliminary tests were conducted at a time frame of 900 s to determine the time to the steady-state (TSS) condition for both the milled and turned conditions. Based on the results, the evolution of the COF during the transient was studied through a time frame of 300 s. Hence, the effect of surface machining processes, i.e., milling and turning, was investigated within this timeframe. The COF evolution was acquired and registered during the test. The vertical displacement of the pin was constantly measured by an LVDT sensor and used as an indication of the wear evolution of the tribological system. Five replicas for each condition were made to obtain statistically representative data and, as stated in ASTM G133-22 standard [25], a new pin was used for each test. The post-processing analysis of the COF evolution to detect the steady-state condition was defined after the comparison of some methods proposed in the literature, i.e., the Moving Standard Deviation (MStD) [26] and the Wavelet transform [27]. According to Cao et al. [28], the R-test algorithm was more effective in steady-state detection; hence, in the present study, a tailed MATLAB$^{\circledR}$ code was developed to determine the TSS and the so-called Ri index was considered to assess deviations from the process variable stability in real time. The Ri index was computed by comparing two variance estimates of the data time series, filtered using adjustable factors, whose calibration dictated the Ri sensitivity to dynamic changes. Ri values were continuously monitored against a threshold, Rcritical, to ascertain steady-state conditions. Thresholds were set based on historical data, considering acceptable variation around the average value. The TSS was determined by the characteristic stabilization times of the variables. The reader is referred to [29] for further details. The above-described numerical method was chosen because of the intrinsic nature of running-in, which can be assumed to be concluded after the stabilization of the COF and the SWR [30,31].

A Talysurf CCILite non-contact 3D profilometer was used to analyze the wear tracks of the disks and calculate their specific wear rate (called SWRd), computed as the ratio between the volume loss and the product of sliding distance and the applied load. The area of the cross-section of the wear track was evaluated on three sections along the wear track and with a scan length, including the wear scar and 2 mm of the unworn surface at both sides. Using TalyMap version 6.2 software (Digital Surf, Besançon, France), flat surfaces were leveled using a least square plane, the filling-in non-measured points filter was applied, and finally, n. 3 profiles were extracted for each acquisition to evaluate the areal measurement. Additionally, the specific wear rates of the pins (called SWRp) were computed by weighing them before and after tests on a Kern ABT 100-5NM (Kern, Balingen, Germany) analytical balance with an accuracy resolution of 0.01. The weighing process was repeated five times through an independent weighing measure process. Then, the weight loss was used to calculate the volume loss by dividing it by the material density, assumed to be equal to 7870 kg/m^3. Lastly, the SWR of the whole tribological system

(called SWRs) was calculated as the sum of the two contributions SWRd and SWRp because of the self-mated tribological pair. The evolution of wear against time was out of the scope of this paper, with the only objective to evaluate the wear rates at the end of the 300 s of the sliding time.

3. Results and Discussion

Figures 2 and 3 display the 3D topographic isometric views of milled and turned samples for all the investigated conditions (M1 to M4 and T1 to T4 from a to d in Figures 1 and 2), respectively. The different reference scales are indicative of the obtained roughness and surface texture. A non-periodical texture was detected in the milled samples when the Ra targeted value increased (Figure 2), while turned surfaces presented regular and equidistant peaks and valleys (Figure 3). Concerning the milled samples, the higher the targeted Ra roughness, the more random the texture (Figure 2) with high peaks and randomly oriented valleys.
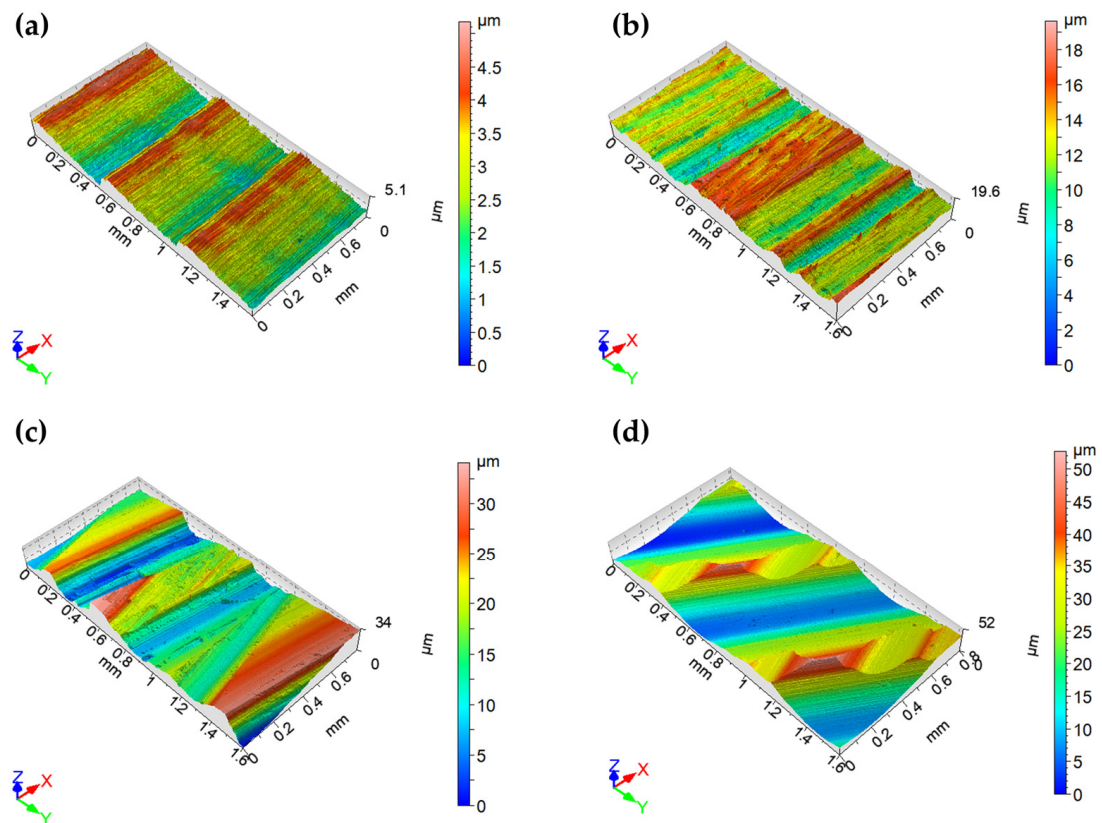

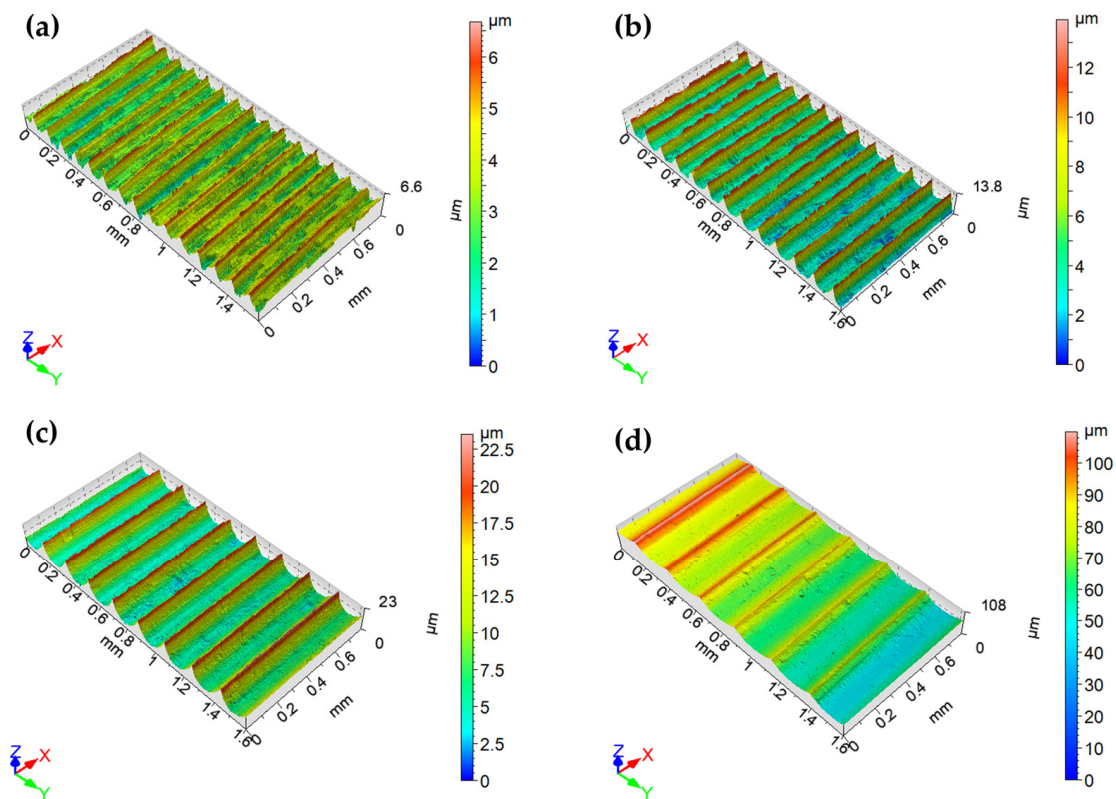**Figure 2.** Three-dimensional topographic isometric views of the milled samples: (**a**) M1, (**b**) M2, (**c**) M3, and (**d**) M4.

Figure 3. Three-dimensional topographic isometric views of the turned samples: (**a**) T1, (**b**) T2, (**c**) T3, and (**d**) T4.

Graphic comparisons of the obtained roughness parameters (Ra, Rq, Rz, Rsk, and Rku) are depicted in Figure 4. It can be noticed that, regarding the 0.8 μm and 1.6 μm targeted values, the turning process led to higher Ra, Rq, and Rz values than the respective milling process for the same targeted 0.8 and 1.6 μm values. On the other hand, for the 3.2 μm and 6.3 μm targeted values, the milled disks exhibited higher Ra, Rq, and Rz values compared to the turned ones. Furthermore, the higher the targeted Ra, the higher the increment in Rz in magnitude, resulting in a surface with a vast difference in peak heights and valley depths (Figure 4a). The Rsk and Rku of each investigated condition are qualitatively reported in Figure 4b. No direct correlation between the two parameters was found in the milled samples, which confirmed the non-periodical nature of the texture. For M1, M2, and M3, the higher the values of the Ra, Rq, and Rz roughness, the lower the Rsk value, while the roughest milled surface (M4) presented the highest Rsk value. Concerning the turned disks, Rsk and Rku decreased with the increase in the targeted Ra, with the only exception of T1, which was characterized by the highest and lowest values of Rsk.
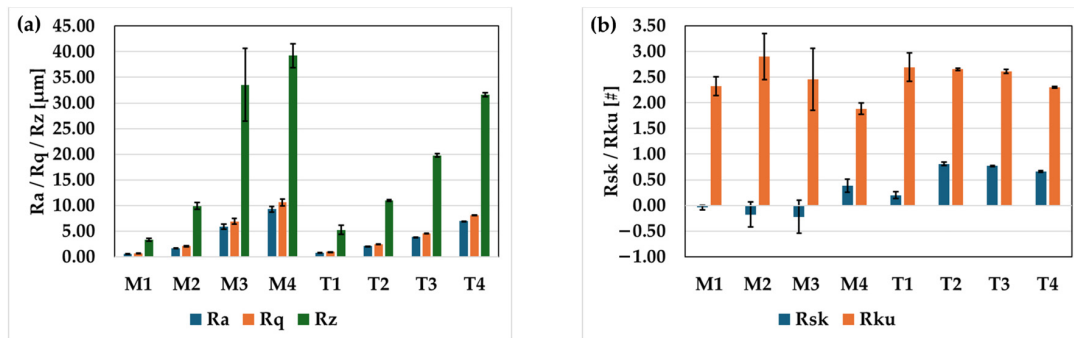

Figure 4. Measured linear roughness parameters for the milled and turned samples: (**a**) Ra, Rq, and Rz and (**b**) Rsk and Rku.

All the Ra, Rq, Rz, Rsk, and Rku roughness values are listed, together with the standard deviations, in Table 2. As it can be seen, the obtained Ra values for all the machined surfaces are coherent with the targeted ones since they were significantly different from one to the other. As a first result, all the roughness parameters for T1 and Pin were very similar, due to the same turning process they underwent. M3 and M4 showed the largest Ra standard deviations (0.50 and 0.56, respectively), reflecting a higher dispersion in the collected data. According to [12], this can be attributed to the pattern produced by the tool during milling, depending on the direction of working/measurement and the eventual overlapping tool path produced during the milling procedure. The same conclusion can be drawn about the Rq and Rz parameters. Gadelmawla et al. [32] stated that Rsk and Rku are useful parameters to better describe surfaces with similar Ra (or Rq) values. Rsk quantifies the symmetry of a profile: a distribution of equal peaks and valleys has zero skewness. A profile with filled-in valleys or high peaks has positive skewness, while profiles with removed peaks or scratches present negative skewness. Furthermore, Rku describes the sharpness of the probability density of the profile. When Rku < 3, the profile shows relatively low high peaks and low valleys; on the other hand, a Rku > 3 distribution is characterized by high peaks and low valleys. For the milled disks, Rku and Rsk did not show any correlation to the corresponding Ra roughness values. Conversely, the turned samples presented a decrease in Rku roughness with the increase in Ra. The T2 disk showed the highest Rsk value. M1 was characterized by the most symmetrical height distribution because of a measured Rsk value closest to 0 (-0.04 ± 0.03 μm), M2 and M3 presented a decreasing trend of the Rsk roughness parameter (-0.18 ± 0.24 and -0.22 ± 0.32 μm, respectively), while M4 showed the highest Rsk value (0.38 ± 0.12 μm) determining a surface with high peaks, as also described by the Rz roughness parameter. These results confirm the surface topography reported in Figure 2. The turned samples were characterized by positive Rsk and Rku values. Especially, it was found that the higher the targeted Ra, the lower the Rku, resulting in an increasing tendency to few high peaks and low valleys.

Table 2. Summary of linear roughness parameters for the milled (M1 to M4) and turned (T1 to T4) disks. Mean values, together with standard deviations, are reported.

	Condition								
Parameter	**M1**	**M2**	**M3**	**M4**	**T1**	**T2**	**T3**	**T4**	**Pin**
Ra [μm]	0.59 ± 0.01	1.69 ± 0.06	5.88 ± 0.50	9.26 ± 0.56	0.77 ± 0.02	2.07 ± 0.01	3.86 ± 0.01	6.93 ± 0.04	0.75 ± 0.01
Rq [μm]	0.71 ± 0.02	2.06 ± 0.09	6.92 ± 0.56	10.60 ± 0.66	0.95 ± 0.03	2.46 ± 0.01	4.60 ± 0.02	8.09 ± 0.05	1.00 ± 0.02
Rz [μm]	3.35 ± 0.31	9.92 ± 0.72	33.53 ± 7.07	39.23 ± 2.35	5.22 ± 0.89	11.0 ± 0.17	19.77 ± 0.32	31.60 ± 0.40	5.04 ± 0.65
Rsk [μm]	-0.04 ± 0.03	-0.18 ± 0.24	-0.22 ± 0.32	0.38 ± 0.12	0.20 ± 0.07	0.81 ± 0.04	0.77 ± 0.01	0.66 ± 0.02	0.16 ± 0.04
Rku [μm]	2.32 ± 0.18	2.90 ± 0.45	2.46 ± 0.60	1.88 ± 0.11	2.69 ± 0.28	2.65 ± 0.02	2.61 ± 0.04	2.30 ± 0.02	2.51 ± 0.26

Figure 5 displays the evolution of the COF as a function of the sliding time obtained by averaging the five replicas. In each curve, a running-in period and a steady-state regime can be observed. The running-in period had different durations depending on both the machining process and the surface roughness. Fluctuations in the COF data can be mainly attributed to adhesion phenomena [33]. It can be observed that, at 1 Hz, the TSS was influenced by the surface roughness both for the milled (Figure 5a) and turned (Figure 5c) disks. In the case of the milled disks (Figure 5a), M4, with the highest roughness, determined the friction curve with the shortest initial transient (running-in) and the lowest fluctuation in the COF value over time. M1 and M3 presented a similar overall behavior, both in terms of the running-in duration and COF data fluctuation. Additionally, in the case of the turned disks (Figure 5c), T1 showed the longest running-in period, while T2 and T3 exhibited the same behavior determining the lowest TSS. Furthermore, at 2 Hz, the running-in periods were similar for the milled samples (Figure 5b) and the turned samples (Figure 5d), except for M4, which was characterized by the highest Ra roughness value. M4 presented the smallest COF fluctuations during running-in, quickly leading to a stable steady-state COF. During the steady-state regime, the COF remained roughly constant in all the selected coupling conditions, reaching similar values for the

same reciprocating frequency (Figure 5a,c and Figure 5b,d, respectively) regardless of the adopted machining process.
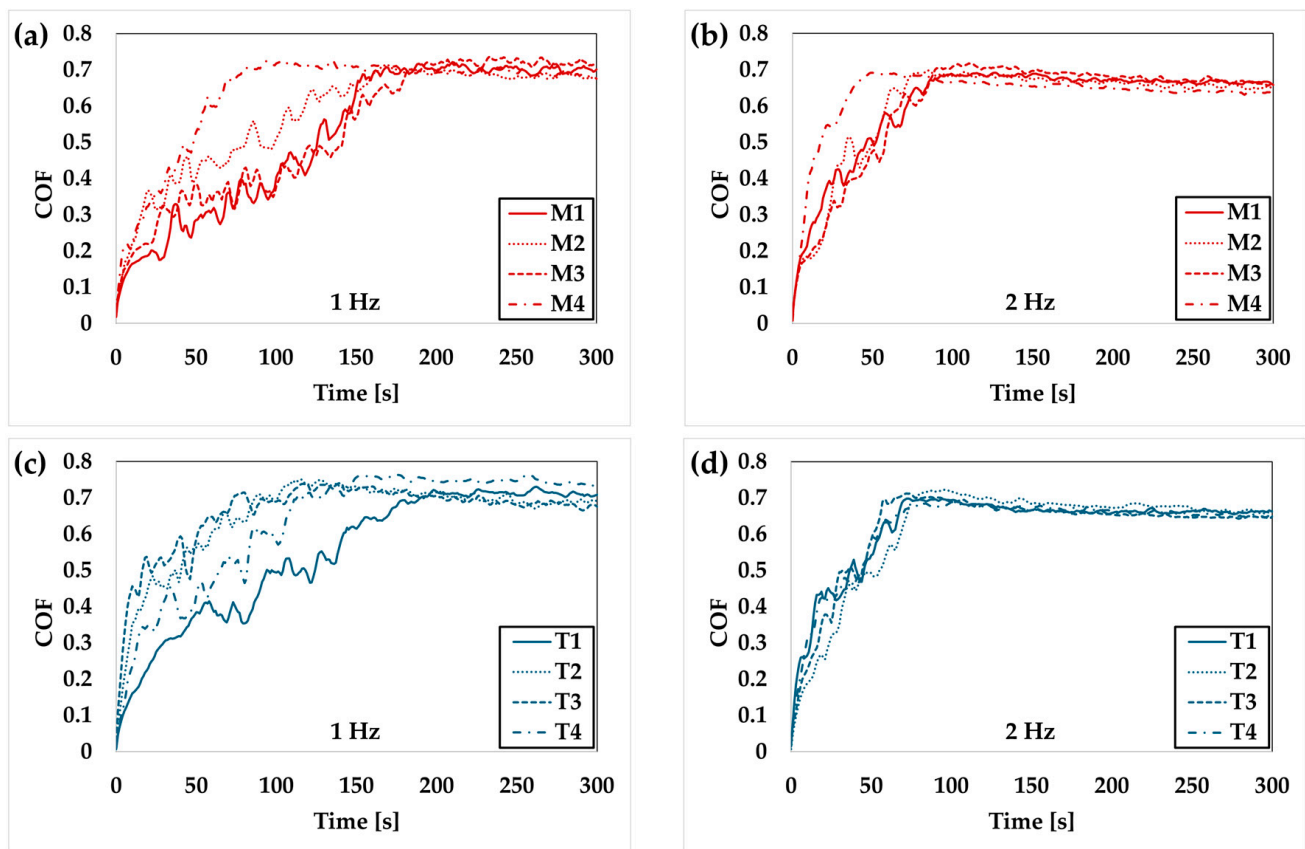

Figure 5. COF evolution during sliding time: (**a**) milled disks at 1 Hz, (**b**) milled disks at 2 Hz, (**c**) turned disks at 1 Hz, and (**d**) turned disks at 2 Hz.

In Figure 6, the overall wear of the investigated tribological systems, measured as vertical displacement at the contact between the two counterbodies during time, is reported. Similarly to the COF evolution, all the curves exhibited a running-in period and later the steady-state wear regime. It must be noticed that, at each reciprocating frequency, all the tribo-couples showed the same system rate of wear in terms of vertical displacements during the steady-state regime, and most of the vertical displacement (i.e., wear of the system) happened in that second half of the test. These findings agree with the COF evolution, which reached the same steady-state value at each reciprocating frequency. At 1 Hz, M4 showed the shortest initial transient (Figure 6a), which was determined by the easier removal of the surface pattern. On the other hand, M1 and M3 presented similar curve slopes, confirming the COF evolution discussed above (Figure 6a). The shorter the wear-in processes for the turned disks (Figure 6c), the higher the overall wear for all the tribological systems. T1 presented the shortest initial transient, while T4 showed the longest one despite the COF evolution depicted in Figure 5c. Nevertheless, the overall wear for the turned disks was minimally affected by the surface roughness of the disks with respect to the milled ones. The same general behavior for the milled and turned disks also emerged at 2 Hz (Figure 6b,d). In the case of the milled disks (Figure 6b), M2 and M3 presented an initial steep increase in the vertical displacement, followed by a slighter increase and the final steady-state overall wear. On the other hand, M1 and M4 showed only the last two steps described. Concerning the turned disks (Figure 6d), all the considered roughness determined similar behaviors with the first steep increase in the overall wear at its minimum in T4, where the Rku was the lowest.
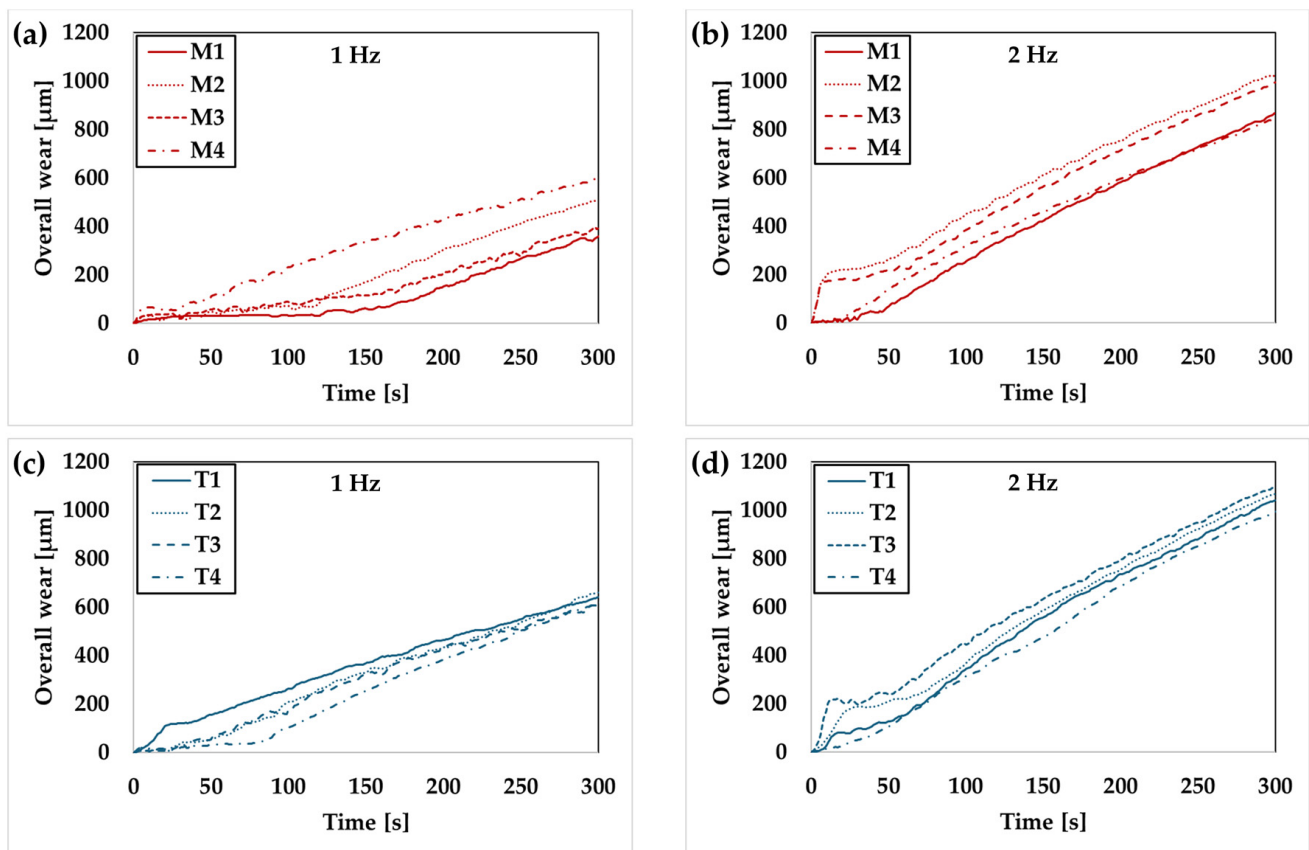
Figure 6. Overall wear evolution during the sliding time: (**a**) milled disks at 1 Hz, (**b**) milled disks at 2 Hz, (**c**) turned disks at 1 Hz, and (**d**) turned disks at 2 Hz.

The average TSS values for the different couplings are reported in Figure 7. As stated by Ba et al. [20], long running-in periods are linked to a low contribution from the adhesive wear between the two counterparts. This behavior was determined by the dimension of the real area contact and the direction of the surface texture with respect to the sliding direction. From Figure 7, it appears that T4 was characterized by the shortest running-in period at 1 Hz, while M4 showed the lowest TSS value at 2 Hz. No linear correlation was found between TSS and the Ra, Rq, and Rz parameters, but it can be noticed that, at 1 Hz, the TSS values were influenced by the Rsk of the respective surfaces. Among the milled disks, M3 showed the minimum TSS value and the lowest Rsk, while the turned T2 disk, with the maximum Rsk value, determined the longest running-in period. In fact, high values of Rsk mean that the surface profile is characterized by high and tight peaks. This leads to a higher contact pressure because of the lower number of total peaks on the disk. When the counterbody slides, the plastic deformation perpendicular to the sliding direction becomes more disadvantaged than the one along the wear track because of the previous sliding cycle [13]. There was no evidence of any correlation between TSS and roughness parameters at the highest reciprocating frequency of 2 Hz.
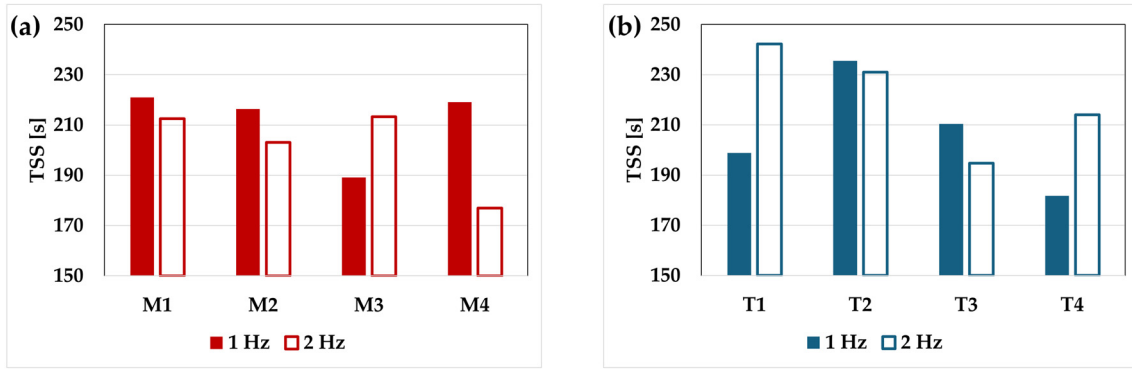
Figure 7. Time to steady-state (TSS) at the investigated reciprocating frequencies of 1 Hz and 2 Hz for the (**a**) milled and (**b**) turned samples.

Figure 8 depicts the SWRd and SWRp values for the different investigated test conditions. Concerning the results obtained with milled disks at 1 Hz, both SWRd and SWRp values increased with the increase in the Ra roughness of the disk, reaching the highest values for the M4 condition. At 2 Hz, SWRp showed the same trend, while SWRd followed the same slope of Rsk roughness parameter, reaching its minimum in M3 (see Figure 3b). In the case of turned samples, SWRp values were higher for each examined roughness at 1 Hz of reciprocating frequency than at 2 Hz, but no significant differences were detected between the different superficial patterns. SWRd appeared to increase with the increase in the Ra, Rq, and Rz roughness values, and it appears to be indirectly proportional to the Rsk (see Figure 3b) at 1 Hz. No correlation could be found for the investigated target roughness at 2 Hz.
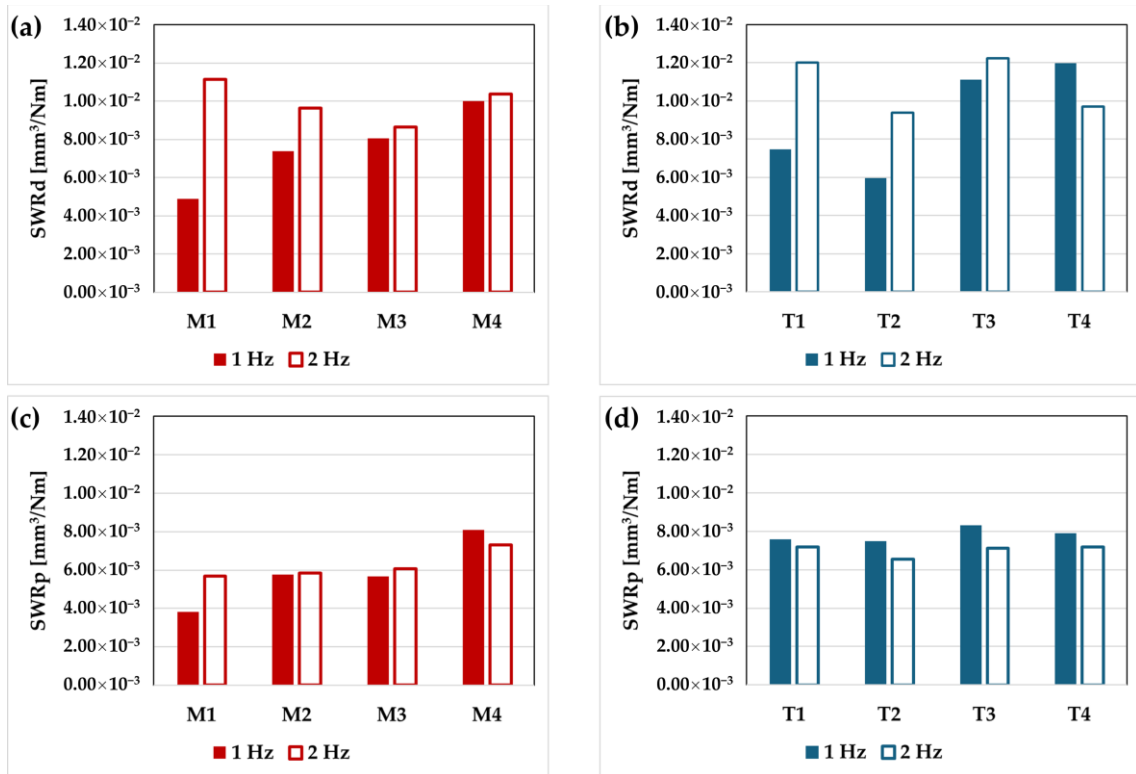

Figure 8. Influence of the reciprocating frequency on (**a**) SWRd for the milled samples, (**b**) SWRd for the turned samples, (**c**) SWRp for the milled samples, and (**d**) SWRp for the turned samples.

Table 3 summarizes the average values and their respective standard deviations of the main tribological parameters, namely COF, TSS, SWRd, SWRp, and the specific wear rate of the tribological system (SWRs). As observed in Figure 5, the lowest COF values were obtained at the highest frequency (i.e., at the highest sliding speed); on the contrary, the highest COF value was shown by the roughest T4 turned disk. These findings agree with the results obtained by [11]. Furthermore, the values were mainly influenced by the reciprocating frequency, showing similar values for all the milled and turned conditions, respectively, at 1 Hz and 2 Hz, in agreement with the results reported in [34]. The calculated standard deviations collected in Table 3 confirmed the good stability of the COF mean value during the reciprocating sliding once the steady-state regime is reached. In this regard, Viáfara [35] related this behavior to the different dynamics of the two bodies: the sliding surface of the rotating disk has intermittent contact while the pin is in constant contact with the surface of the disk, encouraging a higher strain hardening of the pin. This could explain, for all the investigated couplings, the lower SWRp values than their respective SWRd values.

Table 3. Summary of tribological parameters for the milled (M1 to M4) and turned (T1 to T4) samples evaluated at 1 Hz and 2 Hz test conditions. Mean values, together with standard deviations, are reported.

		Condition							
Frequency	Parameter	M1	M2	M3	M4	T1	T2	T3	T4
1 Hz	COF [#]	0.70 ± 0.01	0.68 ± 0.01	0.72 ± 0.01	0.69 ± 0.01	0.71 ± 0.01	0.69 ± 0.01	0.69 ± 0.01	0.75 ± 0.01
	TSS [s]	221 ± 54	216 ± 30	189 ± 40	219 ± 56	199 ± 56	236 ± 45	210 ± 45	182 ± 50
	SWRd [mm^3/Nm]	$4.88 \times 10^{-3} \pm 3.81 \times 10^{-3}$	$7.38 \times 10^{-3} \pm 1.92 \times 10^{-3}$	$8.04 \times 10^{-3} \pm 1.48 \times 10^{-3}$	$1.00 \times 10^{-2} \pm 1.70 \times 10^{-3}$	$7.46 \times 10^{-3} \pm 6.82 \times 10^{-4}$	$5.97 \times 10^{-3} \pm 5.71 \times 10^{-4}$	$1.11 \times 10^{-2} \pm 2.05 \times 10^{-3}$	$1.20 \times 10^{-2} \pm 1.16 \times 10^{-3}$
	SWRp [mm^3/Nm]	$3.81 \times 10^{-3} \pm 5.23 \times 10^{-4}$	$5.76 \times 10^{-3} \pm 7.47 \times 10^{-4}$	$5.68 \times 10^{-3} \pm 2.24 \times 10^{-4}$	$8.08 \times 10^{-3} \pm 7.52 \times 10^{-4}$	$7.57 \times 10^{-3} \pm 1.12 \times 10^{-3}$	$7.49 \times 10^{-3} \pm 9.99 \times 10^{-3}$	$8.32 \times 10^{-3} \pm 8.55 \times 10^{-4}$	$7.90 \times 10^{-3} \pm 1.65 \times 10^{-4}$
	SWRs [mm^3/Nm]	8.69×10^{-3}	1.31×10^{-2}	1.37×10^{-2}	1.81×10^{-2}	1.50×10^{-2}	1.35×10^{-2}	1.94×10^{-2}	1.99×10^{-2}
2 Hz	COF [#]	0.67 ± 0.01	0.66 ± 0.01	0.67 ± 0.01	0.64 ± 0.01	0.66 ± 0.01	0.67 ± 0.01	0.65 ± 0.01	0.65 ± 0.01
	TSS [s]	213 ± 40	203 ± 48	213 ± 38	177 ± 68	242 ± 35	231 ± 38	195 ± 41	214 ± 32
	SWRd [mm^3/Nm]	$1.11 \times 10^{-2} \pm 5.25 \times 10^{-4}$	$9.63 \times 10^{-3} \pm 4.22 \times 10^{-4}$	$8.64 \times 10^{-3} \pm 7.28 \times 10^{-4}$	$1.04 \times 10^{-2} \pm 7.30 \times 10^{-3}$	$1.20 \times 10^{-2} \pm 5.60 \times 10^{-4}$	$9.37 \times 10^{-3} \pm 7.19 \times 10^{-4}$	$1.22 \times 10^{-2} \pm 5.87 \times 10^{-4}$	$9.71 \times 10^{-3} \pm 6.49 \times 10^{-4}$
	SWRp [mm^3/Nm]	$5.68 \times 10^{-3} \pm 9.49 \times 10^{-6}$	$5.83 \times 10^{-3} \pm 1.94 \times 10^{-5}$	$6.06 \times 10^{-3} \pm 2.26 \times 10^{-4}$	$7.30 \times 10^{-3} \pm 8.65 \times 10^{-3}$	$7.19 \times 10^{-3} \pm 2.16 \times 10^{-4}$	$6.56 \times 10^{-3} \pm 8.47 \times 10^{-4}$	$7.13 \times 10^{-3} \pm 2.04 \times 10^{-4}$	$7.19 \times 10^{-3} \pm 7.75 \times 10^{-4}$
	SWRs [mm^3/Nm]	1.68×10^{-2}	1.55×10^{-2}	1.47×10^{-2}	1.77×10^{-2}	1.92×10^{-2}	1.59×10^{-2}	1.94×10^{-2}	1.69×10^{-2}

As the wear rate of the whole system is a valuable control parameter in the case of self-mated materials [35], SWRs were calculated by summing the two contributions from the disk and pin. In the case of the milled samples, at 1 Hz, SWRs increased when the Ra roughness of the disk was higher, while at 2 Hz, the same trend for SWRs and Rsk roughness was found. None of the selected roughness parameters seemed to influence the SWRs of the turned disks at the investigated frequencies. Regardless of the roughness parameters of each surface, an explanation of this behavior was proposed by Bayer et al. [36], who suggested that the orientation of the asperities in the sliding direction of the pin can interfere with the wear behavior. As stated by Ba et al. [20], it is worth mentioning that, when a milled and a turned surface are subjected to the same cutting geometry, feed rate, and cutting depth, the grooves and peaks present on the turned surface will create a preferential path for the wear track, depending on the sliding direction. In the case of the milled samples, the high sharp profile of M4 (with high Rz and Rsk) determined the shortest initial transient (see Figure 6a). This result matches the highest SWRd and SWRp (and SWRs) values, equal to $1.00 \times 10^{-2} \pm 1.70 \times 10^{-3}$ and $8.08 \times 10^{-3} \pm 7.52 \times 10^{-4}$ mm^3/Nm, respectively (and 1.81×10^{-2} mm^3/Nm). This evidence can be attributed to the random direction of the matching of the peaks on the surface of the disk. On the other hand, the turned samples did not affect the SWRp, which was very similar to the different Ra values

at both 1 and 2 Hz (see Figure 8d). In these cases, the sliding always occurred according to the surface texture, and no ridges were met during the 300 s of sliding.

From the perspective of the operational conditions of the damping device, the TSS and SWRs were the two main parameters to be considered and minimized. Based on this, the lowest TSS were statistically determined for M3 and T4 disks at 1 Hz, while concerning SWRs, the best results were obtained for M1 and T2 disks at the same frequency. As concerns the 2 Hz frequency, the lowest TSS values were statistically determined for M4 and T3 disks, while concerning SWRs, the best results were obtained for M3 and T2 disks at the same frequency. Aiming to achieve the best compromise between those two parameters, regardless of the reciprocating frequency, the milled disks were the most effective choice for the development of the mating surfaces of the damping device.

4. Conclusions

The present work investigated the effect of the surface characteristics on the wear properties of structural S355JR steel intended for the development of an innovative seismic device. The interest of this study was the analysis of the COF, SWR, and running-in duration related to the surface roughness characteristics. The paper specifically addressed the impact of the superficial characteristics of eight distinct machined surfaces on the above-mentioned parameters, with the aim of quantifying the wear damage of the seismic damper on a laboratory scale. From the experimental findings, the following conclusions can be drawn:

- Standard roughness parameters Ra, Rq, and Rz, which are commonly used to describe the morphology and quality of surfaces, could not completely explain the wear behavior of the considered application. The testing methodology adopted in this paper seemed to be suitable for demonstrating that Rsk, Rku, and the pattern orientation had an influence on the wear properties of the machined surfaces, as stated also by Ba et al. [20].
- Different roughness characteristics led to a different COF evolution against time. Especially, at 1 Hz, the TSS is influenced by the Rsk roughness for both the milled and turned disks. On the other hand, at 2 Hz, it is not possible to identify any correlation between the TSS and roughness parameters. This is possibly due to the combined effect of the high load and sliding speed and the corresponding time between two consecutive cycles being more effective than the superficial pattern. The steady-state COF was influenced by the reciprocating frequency, showing similar values for the milled and turned disks at 1 Hz and 2 Hz.
- The SWR of disks (SWRd) and pins (SWRp) are influenced mainly by the Ra roughness in the milled samples at 1 Hz: the higher the Ra, the higher the SWR. At 2 Hz, the trend of SWRd is the same as Rsk among the different considered samples. In the case of the turned samples, SWRp is higher for each examined roughness at 1 Hz of reciprocating frequency than at the higher value of 2 Hz. SWRd is inversely proportional to the Rsk (Figure 3b) at 1 Hz, while at 2, Hz no correlation could be found for the investigated target roughness. The obtained SWR values are indicative of a severe wear regime: no final roughness measurements were conducted on the resulting surfaces because of the large amount of wear.
- Hence, at 1 Hz, Rsk roughness is the most important parameter to be controlled to optimize the development of a seismic friction damper device, while at 2 Hz, the selected operating conditions (i.e., 50 N) do not permit to identify any correlation between the tribological outputs and the surfaces' roughness characteristics.
- Aiming to achieve the best compromise between those two parameters, regardless of the reciprocating frequency, the milled disks were the most effective choice for the development of the mating surfaces of the damping device due to their best compromise between TSS and SWRs.

References

1. Titirla, M.D. A State-of-the-Art Review of Passive Energy Dissipation Systems in Steel Braces. *Buildings* **2023**, *13*, 851. [CrossRef]
2. Soffritti, C.; Merlin, M.; Vazquez, R.; Garagnani, G.L. Tribological Behavior of a Cr_2O_3 Ceramic Coating/Steel Couple Under Dry Sliding and Heavy Loading Conditions. *J. Mater. Eng. Perform.* **2018**, *27*, 3699–3708. [CrossRef]
3. Merlin, M.; Soffritti, C.; Vazquez, R. Effect of relative humidity and applied loads on the tribological behaviour of a steel/Cr_2O_3-ceramic coupling. *Wear* **2013**, *303*, 371–380. [CrossRef]
4. Franceschi, M.; Soffritti, C.; Fortini, A.; Pezzato, L.; Garagnani, G.L.; Dabalà, M. Evaluation of wear resistance of a novel carbide-free bainitic steel. *Tribol. Int.* **2023**, *178*, 108071. [CrossRef]
5. Sedlaček, M.; Gregorčič, P.; Podgornik, B. Use of the Roughness Parameters S sk and S ku to Control Friction—A Method for Designing Surface Texturing. *Tribol. Trans.* **2017**, *60*, 260–266. [CrossRef]
6. Sedlaček, M.; Podgornik, B.; Vižintin, J. Planning surface texturing for reduced friction in lubricated sliding using surface roughness parameters skewness and kurtosis. *Proc. Inst. Mech. Eng. Part J J. Eng. Tribol.* **2012**, *226*, 661–667. [CrossRef]
7. Costa, H.; Hutchings, I. Some innovative surface texturing techniques for tribological purposes. *Proc. Inst. Mech. Eng. Part J J. Eng. Tribol.* **2015**, *229*, 429–448. [CrossRef]
8. Nsilani Kouediatouka, A.; Ma, Q.; Liu, Q.; Mawignon, F.J.; Rafique, F.; Dong, G. Design Methodology and Application of Surface Texture: A Review. *Coatings* **2022**, *12*, 1015. [CrossRef]
9. Sinha, A.; Ischia, G.; Menapace, C.; Gialanella, S. Experimental Characterization Protocols for Wear Products from Disc Brake Materials. *Atmosphere* **2020**, *11*, 1102. [CrossRef]
10. Kubiak, K.J.; Liskiewicz, T.W.; Mathia, T.G. Surface morphology in engineering applications: Influence of roughness on sliding and wear in dry fretting. *Tribol. Int.* **2011**, *44*, 1427–1432. [CrossRef]
11. Sedlaček, M.; Podgornik, B.; Vižintin, J. Correlation between standard roughness parameters skewness and kurtosis and tribological behaviour of contact surfaces. *Tribol. Int.* **2012**, *48*, 102–112. [CrossRef]
12. Sedlaček, M.; Podgornik, B.; Vižintin, J. Influence of surface preparation on roughness parameters, friction and wear. *Wear* **2009**, *266*, 482–487. [CrossRef]
13. Liang, G.; Schmauder, S.; Lyu, M.; Schneider, Y.; Zhang, C.; Han, Y. An Investigation of the Influence of Initial Roughness on the Friction and Wear Behavior of Ground Surfaces. *Materials* **2018**, *11*, 237. [CrossRef]
14. Pawlus, P.; Reizer, R.; Wieczorowski, M. Functional Importance of Surface Texture Parameters. *Materials* **2021**, *14*, 5326. [CrossRef] [PubMed]
15. Wang, B.; Zheng, M.; Zhang, W. Analysis and Prediction of Wear Performance of Different Topography Surface. *Materials* **2020**, *13*, 5056. [CrossRef] [PubMed]
16. Grzesik, W. Prediction of the Functional Performance of Machined Components Based on Surface Topography: State of the Art. *J. Mater. Eng. Perform.* **2016**, *25*, 4460–4468. [CrossRef]
17. Elwasli, F.; Mzali, S.; Zemzemi, F.; Mezlini, S. Numerical Simulation of Reciprocating Sliding Test: Effects of Surface Topography on the Wear Behavior. In *Advances in Mechanical Engineering, Materials and Mechanics, Proceedings of the 7th International Conference on Advances in Mechanical Engineering and Mechanics, Hammamet, Tunisia, 16–18 December 2019*; Springer: Cham, Switzerland, 2021; pp. 240–245.
18. Prajaapti, D.K. Surface Topography Evolution of Engineered Surfaces during Sliding Wear. *Key Eng. Mater.* **2021**, *901*, 199–207. [CrossRef]

19. Kuang, W.; Miao, Q.; Ding, W.; Li, H. A short review on the influence of mechanical machining on tribological and wear behavior of components. *Int. J. Adv. Manuf. Technol.* **2022**, *120*, 1401–1413. [CrossRef]

20. Ba, E.C.T.; Dumont, M.R.; Martins, P.S.; Drumond, R.M.; Martins da Cruz, M.P.; Vieira, V.F. Investigation of the effects of skewness Rsk and kurtosis Rku on tribological behavior in a pin-on-disc test of surfaces machined by conventional milling and turning processes. *Mater. Res.* **2021**, *24*, e20200435. [CrossRef]

21. Grossi, E.; Baroni, E.; Aprile, A.; Fortini, A.; Zerbin, M.; Merlin, M. Tribological Behavior of Structural Steel with Different Surface Finishing and Treatments for a Novel Seismic Damper. *Coatings* **2023**, *13*, 135. [CrossRef]

22. Grossi, E.; Aprile, A.; Zerbin, M. Tribological investigation on metal mating surfaces to explore real use conditions of a novel friction damper for seismic applications. *Eng. Struct.* **2023**, *278*, 115473. [CrossRef]

23. *ISO 4287:1997*; Geometrical Product Specifications (GPS)—Surface Texture: Profile Method—Terms, Definitions and Surface Texture Parameters. International Organization for Standarization: Geneva, Switzerland, 1997.

24. *ASTM G. 99–95a*; Standard Test Method for Wear Testing with a Pin-on-Disk Apparatus. ASTM International: West Conshohocken, PA, USA, 2000.

25. *ASTM G. 133*; Standard Test Method for Linearly Reciprocating Ball-on-Flat Sliding Wear. ASTM International: West Conshohocken, PA, USA, 2016.

26. Kim, M.; Yoon, S.H.; Domanski, P.A.; Vance Payne, W. Design of a steady-state detector for fault detection and diagnosis of a residential air conditioner. *Int. J. Refrig.* **2008**, *31*, 790–799. [CrossRef]

27. Jiang, T.; Chen, B.; He, X.; Stuart, P. Application of steady-state detection method based on wavelet transform. *Comput. Chem. Eng.* **2003**, *27*, 569–578. [CrossRef]

28. Cao, S.; Rhinehart, R.R. Critical values for a steady-state identifier. *J. Process Control* **1997**, *7*, 149–152. [CrossRef]

29. Bianchi, M.; Branchini, L.; Casari, N.; De Pascale, A.; Melino, F.; Ottaviano, S.; Pinelli, M.; Spina, P.R.; Suman, A. Experimental analysis of a micro-ORC driven by piston expander for low-grade heat recovery. *Appl. Therm. Eng.* **2019**, *148*, 1278–1291. [CrossRef]

30. Blau, P.J. Running-in: Art or engineering? *J. Mater. Eng.* **1991**, *13*, 47–53. [CrossRef]

31. Blau, P.J. How common is the steady-state? The implications of wear transitions for materials selection and design. *Wear* **2015**, *332–333*, 1120–1128. [CrossRef]

32. Gadelmawla, E.S.; Koura, M.M.; Maksoud, T.M.A.; Elewa, I.M.; Soliman, H.H. Roughness parameters. *J. Mater. Process. Technol.* **2002**, *123*, 133–145. [CrossRef]

33. Okonkwo, P.C.; Kelly, G.; Rolfe, B.F.; Pereira, M.P. The effect of sliding speed on the wear of steel–tool steel pairs. *Tribol. Int.* **2016**, *97*, 218–227. [CrossRef]

34. Blau, P.J. On the nature of running-in. *Tribol. Int.* **2005**, *38*, 1007–1012. [CrossRef]

35. Viáfara, C.C.; Sinatora, A. Influence of hardness of the harder body on wear regime transition in a sliding pair of steels. *Wear* **2009**, *267*, 425–432. [CrossRef]

36. Bayer, R.G.; Sirico, J.L. The influence of surface roughness on wear. *Wear* **1975**, *35*, 251–260. [CrossRef]